Hindawi
Adsorption Science & Technology
Volume 2022, Article ID 3207986, 12 pages
https://doi.org/10.1155/2022/3207986

*Research Article*

# Enhanced $CO_2$ Adsorption and Selectivity of $CO_2/N_2$ on Amine@ZIF-8 Materials

**Zhijuan Zhang**,[1,2] **Pengwei Li**,[1] **Ting Zhao**,[1] **and Yuanhan Xia**[2]

[1]*College of Pharmacy, Henan University of Chinese Medicine, Zhengzhou 450046, China*
[2]*Institute of Mass Spectrometer and Atmospheric Environment, Jinan University, Guangzhou 510632, China*

Correspondence should be addressed to Zhijuan Zhang; zhangyan0204@126.com

Received 30 September 2021; Revised 31 December 2021; Accepted 4 February 2022; Published 17 February 2022

Academic Editor: Eloy S. Sanz P rez



The ZIF-8 crystals were successfully postsynthetically modified using methylamine (MA), ethylenediamine (ED), and *N*, *N* ′ -dimethylethylenediamine (MMEN) to improve their adsorption performance toward $CO_2$. Results showed that, compared with the original ZIF-8, the BET specific surface area of MA-ZIF-8, MMEN-ZIF-8, and ED-ZIF-8 has increased by 118.2%, 92.0%, and 29.8%, respectively. In addition, their total pore volume increased separately by 130.8%, 100%, and 48.7%. The adsorption capacities of $CO_2$ on the amine-modified ZIF-8 samples followed the order MA − ZIF − 8 > MMEN − ZIF − 8 > ED − ZIF − 8 > ZIF − 8. The $CO_2$ adsorption capacities at 298 K on MA-ZIF-8, MMEN-ZIF-8, and ED-ZIF-8 were increased by 118.2%, 90.2%, and 29.8%, respectively. What is more, the $CO_2/N_2$ selectivities calculated using an IAST model of the amine@ZIF-8 samples at 0.01 bar and 298 K were also significantly improved and followed the order MA − ZIF − 8 (31.4) > ED − ZIF − 8 (25.1) > MMEN − ZIF − 8 (14.1) > ZIF − 8 (11.5), which increased by 173.0%, 121.4%, and 22.6%, respectively. The isosteric heat of $CO_2$ adsorption ($Q_{st}$) on the MA-ZIF-8, MMEN-ZIF-8, and ED-ZIF-8 all becomes higher, while $Q_{st}$ of $N_2$ on these samples was slightly lower in comparison with that on the ZIF-8. Furthermore, after six recycle runs of gravimetric $CO_2$ adsorption-desorption on MA-ZIF-8, the adsorption performance of $CO_2$ is still very good, indicating that the MA-ZIF-8 sample has good regeneration performance and can be applied into industrial $CO_2$ adsorption and separation.

## 1. Introduction

Nowadays, the rising level of carbon dioxide in the atmosphere has become one of the biggest problems worldwide. As the main component of greenhouse gases, $CO_2$ contributes the most to global warming and climate change [1]. To date, the global $CO_2$ concentration has increased from 270 to 400 ppm with the industrial development and is anticipated to approach 950 ppm by 2100, which will bring about sincere environmental problems such as extreme weather, glacial melting, and ocean acidification [2, 3]. Therefore, reducing carbon dioxide emission has been proposed to be a scientific challenge of the highest order and thus has been explored by many researchers throughout the world utilizing different technologies [4–7]. Among these technologies, chemical absorption with aqueous organic amines like diethanolamine (DEA) has been widely used for $CO_2$ capture from industrial waste gases for some time, but they are still subject to volatilization or degradation of organic amines, instrument corrosion, and high energy consumption for solvent regeneration [8–10]. Therefore, adsorption technology using various kinds of solid porous adsorbents has been proposed for $CO_2$ capture and separation.

Different types of adsorbents have been investigated and developed for $CO_2$ adsorption, for example, carbon-based materials, zeolites, metal oxides, and mesoporous silica [7, 11–18]. Nevertheless, these conventional porous materials usually display limited performance toward $CO_2$ adsorption capacity as well as selectivity. Metal-Organic frameworks (MOFs) composed of metal ions and organic linkers, also known as porous coordination polymers, have developed rapidly and attracted significant attentions in the past two decades [19–26]. Owing to their diverse framework structure, high crystallinity, large surface area, and unlimited adjustability of pore structures and surface functionalities, MOFs exhibit great application prospects in the field of

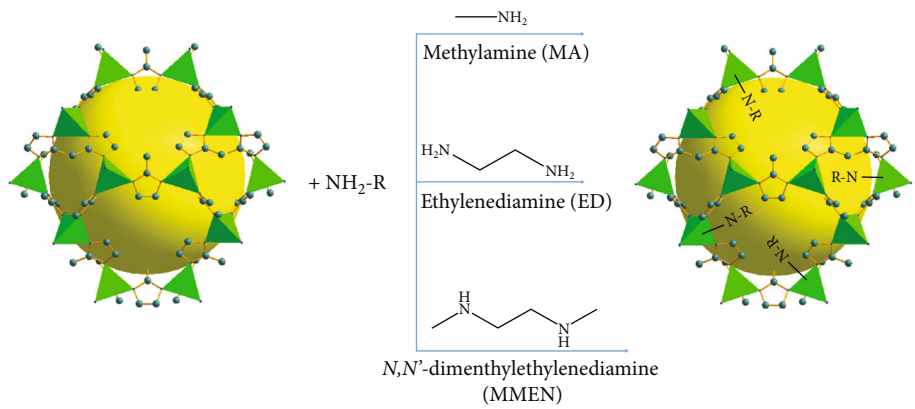


Scheme 1: Preparation of amine-functionalized ZIF-8 using three different amines.

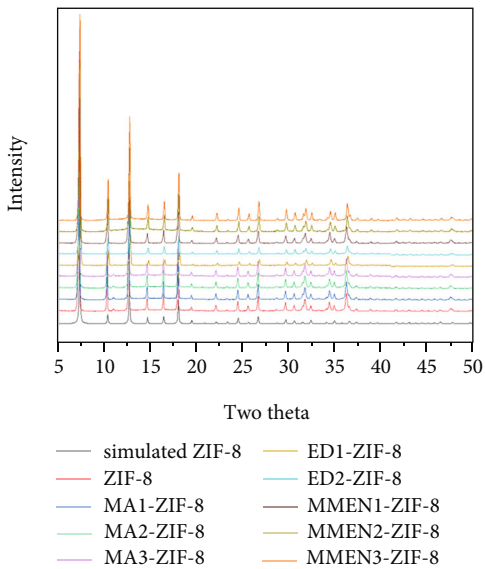


Figure 1: PXRD patterns of ZIF-8 and amine-modified ZIF-8 samples.

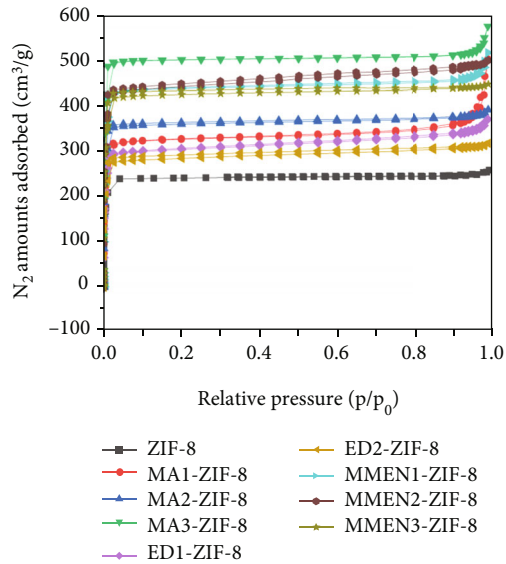


Figure 2: $N_2$ adsorption-desorption isotherms of modified ZIF-8 samples at 77 K.

$CO_2$ capture [14, 15, 21, 23, 27–37]. Nevertheless, it still remains a challenge to design MOFs with quite high $CO_2/N_2$ selectivity as well as $CO_2$ adsorption capacity since the large surface area of MOFs usually leads to both increased $CO_2$ and $N_2$ adsorption capacities, resulting in limited $CO_2/N_2$ adsorption selectivity.

Many researches have tried to improve both the $CO_2$ adsorption capacity and selectivity of MOFs, for instance, ligand functionalization [38, 39], incorporation of open metal sites [29, 40, 41], construction of specific pores [17], and pre-/postmodification for amine grafting/impregnation [36, 42–48]. Zhu et al. [42] reported that the polyethyleneimine-modified UiO-66-$NH_2$ (Zr) exhibited a considerable enhancement toward $CO_2/N_2$ adsorption selectivity (48 vs. 25) and moderate desorption energy (68 kJ/mol $CO_2$). Additionally, Justin et al. [49] described that the tris (2-aminoethyl) amine- (TAEA-) appended-$Zn_4O$ $(NH_2\text{-}BDC)_{1.2}(BrAcNH\text{-}BDC)_{1.8}$ displayed a dramatically increased $CO_2/N_2$ (15/85) selectivity (143) at 313 K and a zero-coverage $Q_{st}$ of $CO_2$ adsorption of 62.5 kJ/mol. However, the high heat of adsorption owing to the strong interaction usually signifies high energy for adsorbent regeneration process. Thus, the development of adsorbents with high $CO_2$ adsorption capacity, $CO_2/N_2$ selectivity, moderate energy consumption, and good stability still remains a challenge for real application.

In the current work, in order to improve its $CO_2$ adsorption capacity and $CO_2/N_2$ selectivity, the ZIF-8 will be post-synthetically modified by using methylamine (MA), ethylenediamine (ED), and *N*, *N* ′-dimethylethylenediamine (MMEN) to obtain a series of novel amine@ZIF-8 materials. Then, the pore structure, PXRD, surface chemistry, and thermogravimetric stability of the prepared amine@ZIF-8 materials would be characterized. The pure-component $CO_2$ and $N_2$ isotherms on the amine@ZIF-8 would be measured separately at ambient temperatures. In

Table 1: Texture properties of the amine-modified ZIF-8 samples.

| Samples | $S_{BET}$ ($m^2$/g) | $V_{micro}$ ($cm^3$/g) | Average diameter (Å) | $V_{total}$ ($cm^3$/g) |
|---|---|---|---|---|
| ZIF-8 | 1038 | 0.37 | 14.92 | 0.39 |
| MA1-ZIF-8 | 1435 | 0.49 | 21.91 | 0.79 |
| MA2-ZIF-8 | 2265 | 0.78 | 15.88 | 0.90 |
| MA3-ZIF-8 | 1545 | 0.54 | 16.06 | 0.62 |
| ED1-ZIF-8 | 1347 | 0.44 | 17.19 | 0.58 |
| ED2-ZIF-8 | 1257 | 0.43 | 15.77 | 0.50 |
| MMEN1-ZIF-8 | 1963 | 0.67 | 16.47 | 0.81 |
| MMEN2-ZIF-8 | 1994 | 0.65 | 15.69 | 0.78 |
| MMEN3-ZIF-8 | 1899 | 0.65 | 14.74 | 0.70 |

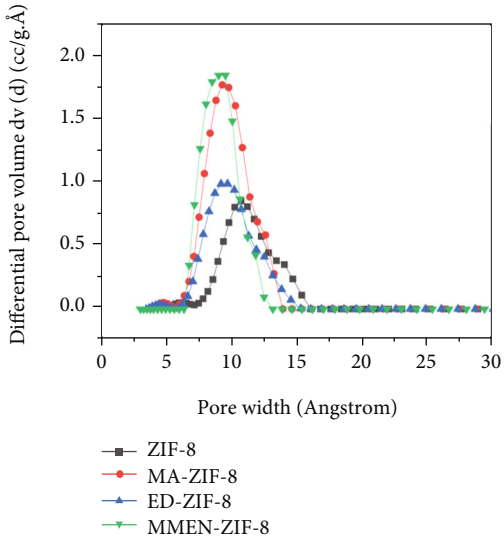


Figure 3: DFT pore size distribution for ZIF-8 and amine-modified ZIF-8 materials.

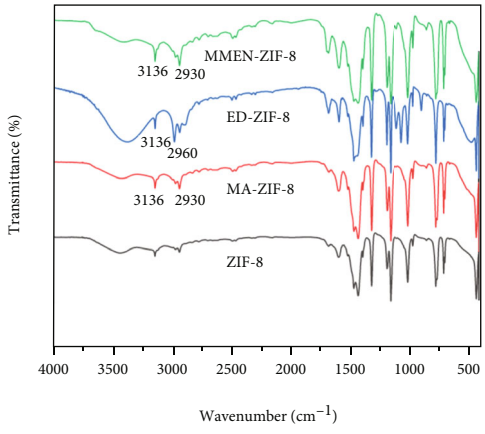


Figure 4: FTIR spectra of MA-ZIF-8, ED-ZIF-8, and MMEN-ZIF-8.

addition, the equimolar $CO_2/N_2$ selectivity is estimated by using an ideal adsorbed solution theory (IAST) model. Moreover, the $Q_{st}$ of $CO_2$ adsorption on the amine@ZIF-8 was calculated. Finally, the reusability of amine@ZIF-8 toward $CO_2$ adsorption was also investigated. The multiple gravimetric adsorption-desorption performance is expected to provide an application basis for industrial $CO_2$ capture.

## 2. Materials and Methods

*2.1. Materials.* Zn $(NO_3)_2 \cdot 6H_2O$ (Alfa Aesar, 99.99% purity), was purchased from Alfa Aesar Chemical; 2-methylimidazole (98% purity), *N*, *N* ′-dimethylformamide (99.9%), anhydrous methanol (99.8%), ammonia (analytical pure), methylamine (analytical pure), and *N*, *N* ′-dimethylethylenediamine (97%)were bought from J&K Chemical; chloroform (analytical pure) was obtained from Guangzhou Chemical Reagent Factory; and ethylenediamine (≥99.5%) was purchased from Aladdin.

*2.2. Synthesis and Modification.* Preparation and amine modification of ZIF-8 were carried out according to the reported procedures with a few modifications [50, 51]. The concentration gradients of methylamine (MA), ethylenediamine (ED), and *N*, *N* ′-dimethylethylenediamine (MMEN) used are listed in Table S1. In this work, the MA-modified ZIF-8 with different concentrations were named as MA1-ZIF-8, MA2-ZIF-8, etc. The name of ED-modified ZIF-8 and MMEN-modified ZIF-8 was in the same manner.

*2.3. Characterization.* The PXRD patterns were obtained by an X-ray diffractometer (D8 advance, Bruker) using Cu K$\alpha$ line focused radiation (wavelength $\lambda = 0.15406$ nm). The chemical bonds and surface organic groups were observed using a FTIR spectrophotometer (Bruker TENSOR II Apparatus, Bruker Optics Inc., Germany). The thermal stability was characterized by using a thermogravimetric analyzer (TA-550 apparatus, TA Instruments, USA). The porous structures were analysed using a Quantachrome Autosorb IQ2 instrument. All the tested samples were degassed at 473 K under vacuum overnight.

*2.4. $CO_2$ and $N_2$ Adsorption Isotherms at Ambient Temperature.* The specific adsorbed amounts of pure $CO_2$ and $N_2$ were measured using a static volumetric method on the Quantachrome Autosorb IQ2 instrument at three temperatures (273 K, 288 K, and 298 K, respectively). The initial activation of amine@ZIF-8 materials was performed at 523 K for 8 h under vacuum. Helium (ultrahigh purity) was the purge gas; $CO_2$ and $N_2$ were both of 99.999% purities.

*2.5. Reusability Assessment.* The regeneration performance was studied to evaluate the recyclability of the amine@ZIF-8. In this study, both volumetric and gravimetric adsorption-desorption cycles were carried out. For the volumetric experiments, multiple $CO_2$ adsorption-desorption cycles on amine@ZIF-8 were operated by the Quantachrome Autosorb IQ2 instrument at 298 K. During each cycle, the maximum adsorption pressure was set at 1 bar; while the minimum

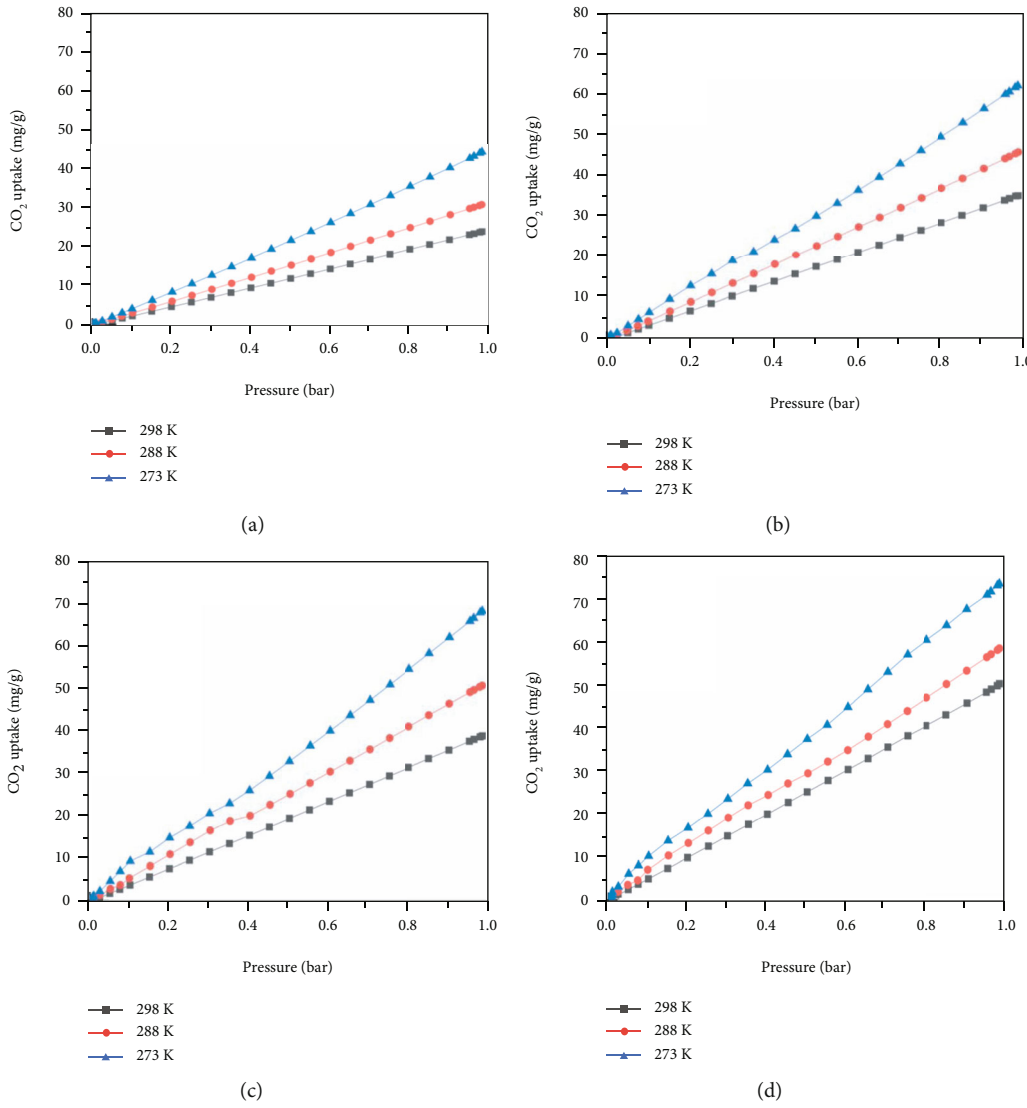


Figure 5: The $CO_2$ adsorption isotherms on the amine@ZIF-8 materials at 273 K, 288 K, and 298 K. (a) ZIF-8; (b) MA-ZIF-8; (c) ED-ZIF-8; (d) MMEN-ZIF-8.

desorption pressure was 1 mbar. The whole desorption process was under vacuum at 473 K for 8 h. For the gravimetric method, the six adsorption-desorption cycles were determined on a TA550 system under different regeneration temperatures (125°C and 150°C, respectively) [52, 53]. Before the recycle experiment, 5 mg of modified ZIF-8 sample was put in a platinum pan and heated to 150°C with a speed of 10°C/min and under high-purity $N_2$ (99.999%, 60 mL/min) to desorb any preadsorbed gases on the surfaces of the sample. Then, the sample was retained under $N_2$ atmosphere until a constant weight was reached at 25°C. After that, the gas was switched to a $CO_2/N_2$ mixture stream (60 mL/min of total flow, 90% $CO_2$, balance $N_2$) and kept for 30 min.

## 3. Results and Discussion

*3.1. Characterization of Amine@ZIF-8 Materials.* The post-synthetic modification route is demonstrated in Scheme 1. The amount of amine grafted on the ZIF-8 material is the key factor that may greatly affect its porous structure. Figure 1 shows the PXRD patterns of amine@ZIF-8 materials. Clearly, the modified ZIF-8 materials all show diffraction peaks at 7.29°, 10.32°, 12.65°, 16.50°, and 18.01°. These peaks are the same as the characteristics of the diffraction spectrum of the original ZIF-8. The peak positions are also consistent as compared to the simulated ZIF-8, implying that amine@ZIF-8 materials still maintain a complete crystal structure without structural collapse [30].

Figure 2 depicts the $N_2$ adsorption-desorption isotherms at 77 K on amine@ZIF-8 materials. Obviously, the tested amine@ZIF-8 materials all presented typical type I behaviour, suggesting that there were mainly micropores in nature. Interestingly, hystereses were observed for the amine@ZIF-8 samples in the pressure range of 0.96-1.0. These hystereses were ascribed to the formed pores between the gaps of modified ZIF-8 particles, not owing to the mesopores.

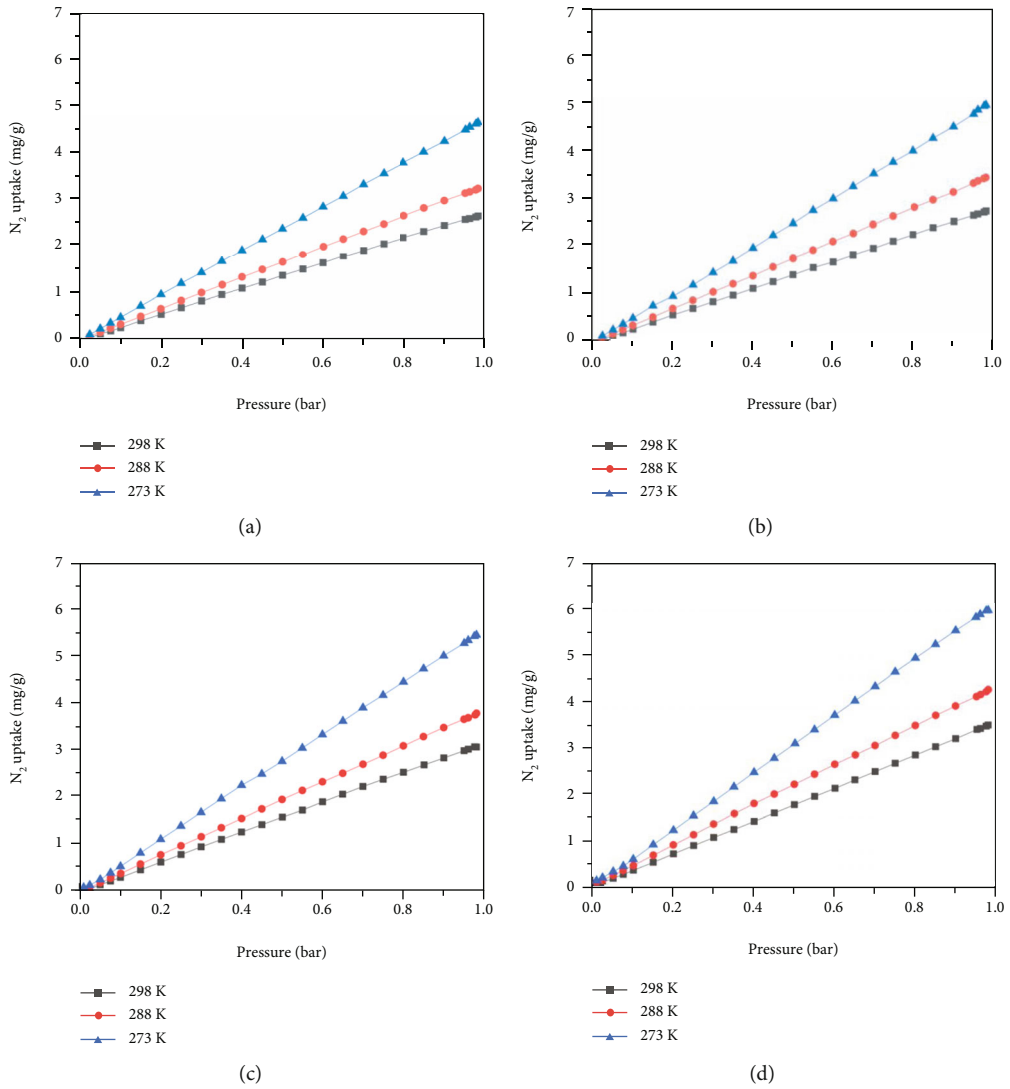


Figure 6: The $N_2$ adsorption isotherms on the amine@ZIF-8 materials at 273 K, 288 K, and 298 K. (a) ZIF-8; (b) MA-ZIF-8; (c) ED-ZIF-8; (d) MMEN-ZIF-8.

Table 1 lists the parameters of porous structures for amine@ZIF-8. It can be seen that with the increase of MA, ED, and MMEN, the BET specific surface areas all showed a trend of first increasing and then decreasing. In addition, the total pore volume also presented the same trend as well as the micropore volume. Compared with the original ZIF-8, the BET specific surface areas of MA2-ZIF-8, MMEN2-ZIF-8, and ED1-ZIF-8 increased by 118.2%, 92.0%, and 29.8%, respectively. Furthermore, their total pore volume increased separately by 130.8%, 100%, and 48.7%. Moreover, the micropore volumes of MA2-ZIF-8, MMEN2-ZIF-8, and ED1-ZIF-8 raised separately by 110.8%, 75.7%, and 18.9%. Thereafter, the MA2-ZIF-8, ED1-ZIF-8, and MMEN2-ZIF-8 can be recognized as the three best samples among the amine@ZIF-8 materials, and they would be marked as MA-ZIF-8, ED-ZIF-8, and MMEN-ZIF-8, respectively, in the following adsorption experiments. However, it should be pointed out that the BET surface area of the as-made ZIF-8 was lower than that synthesized by Park et al. [54], but still in the range of the reported ZIF-8 (see Table S2). This, possibly, indicated that the prepared ZIF-8 in this work still contained some residual species in the cavities (e.g., $CHCl_3$, DMF, or unreacted Hmim) which could not desorbed during the activated step. In addition, the different results between these three amine@ZIF-8 samples were probably owing to the different reactivities of amines. Therefore, the reason of the increases of the BET surface area and pore volume might be that, after the postsynthetic modification, some occlusive pores of the ZIF-8 were reopened, and more new pores were formed at meanwhile [45]. Nevertheless, when the loading amount of MA, ED, and MMEN added further, the surface areas and pore volumes begun to decrease because of hindrance effect of the introduced amines [55, 56].

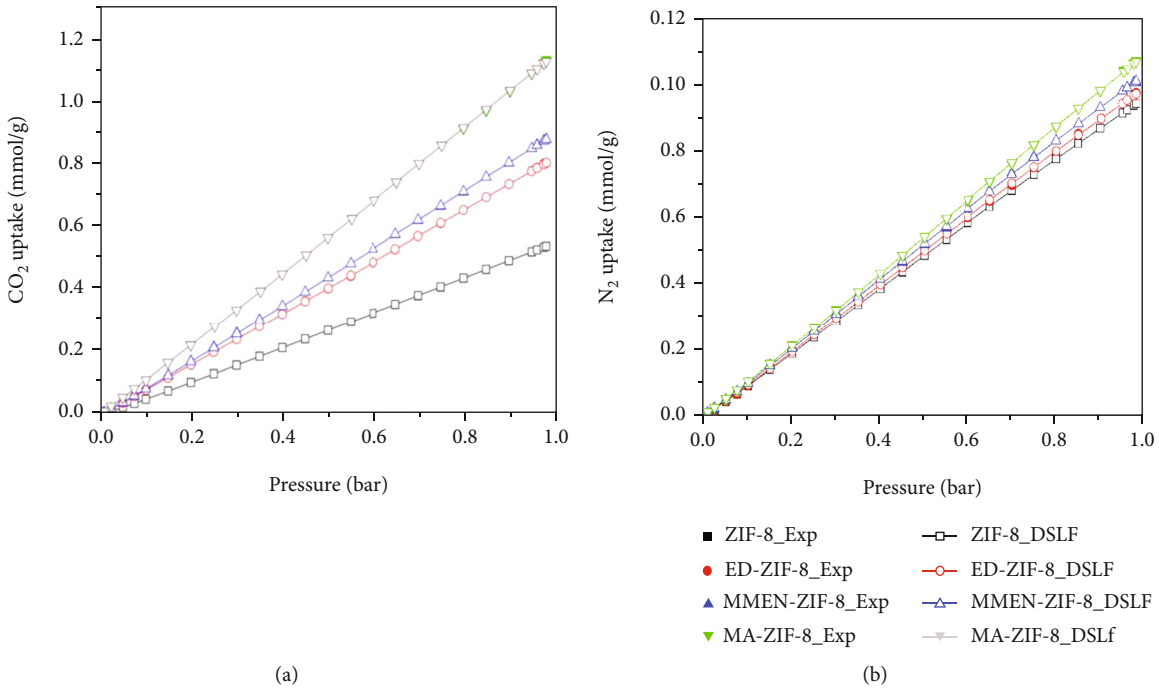


Figure 7: DSLF fitting of the $CO_2$ and $N_2$ isotherms on the amine@ZIF-8 at 298 K: (a) $CO_2$; (b) $N_2$.

Table 2: The fitting parameters of the DLSF model for the pure component isotherms of $CO_2$ and $N_2$ at 298 K.

| | ZIF-8 | | MA-ZIF-8 | | ED-ZIF-8 | | MMEN-ZIF-8 | |
|---|---|---|---|---|---|---|---|---|
| | $CO_2$ | $N_2$ | $CO_2$ | $N_2$ | $CO_2$ | $N_2$ | $CO_2$ | $N_2$ |
| $R^2$ | 0.9999 | 0.9999 | 0.9999 | 0.9999 | 0.9999 | 0.9999 | 0.9999 | 0.9999 |
| $q_{m,1}$ (mmol/g) | 9.603 | 0.4885 | 31.29 | 1.162 | 25.40 | 0.5662 | 25.51 | 0.6675 |
| $q_{m,2}$ (mmol/g) | 0.8383 | 0.1881 | 2.546 | 0.2749 | 2.053 | 0.1524 | 3.318 | 0.1175 |
| $b_1$ ($kPa^{-1}$) | 0.0004380 | 0.001094 | 0.0002336 | 0.0005896 | 0.0002480 | 0.001083 | 0.0001730 | 0.001058 |
| $b_2$ ($kPa^{-1}$) | 0.0001580 | 0.0008590 | 0.001621 | 0.0005974 | 0.0007272 | 0.0007152 | 0.0008817 | 0.0006616 |
| $n_1$ | 0.9304 | 0.8905 | 0.9209 | 0.9342 | 0.9453 | 0.9039 | 0.9223 | 0.9155 |
| $n_2$ | 1.867 | 0.9500 | 1.328 | 1.104 | 1.382 | 0.9077 | 0.9883 | 0.9011 |

Figure S1 exhibits the DFT pore size distributions of ZIF-8 and amine@ZIF-8 materials. Apparently, for each MA-ZIF-8, MMEN-ZIF-8, and ED-ZIF-8 material, the main pore size was lower than that of the as-made ZIF-8. Figure 3 demonstrates the DFT pore size distributions for the best amine@ZIF-8 materials. It can be noticed that the main pore size of the original ZIF-8 is distributed at 10.87 Å, while those of the MA-ZIF-8, ED-ZIF-8, and MMEN-ZIF-8 are distributed at around 9.26 Å, suggesting that the introduction of an amine group would result in reduced pore size [47]. This might be due to the new formed pores with the introduction of MA, ED, and MMEN, respectively. The reduced pore size also indicated that there were mainly micropores in the amine@ZIF-8 frameworks.

Figure 4 illustrates the infrared spectra of amine@ZIF-8 materials. First of all, the infrared spectra of amine@ZIF-8 materials were basically similar to those of ZIF-8. Secondly, the peak intensities of MA-ZIF-8 and ED-ZIF-8 material at around 3136 $cm^{-1}$ were significantly enhanced, and at 2960 $cm^{-1}$ and 2930 $cm^{-1}$, the intensities of the antisymmetric stretching vibration peaks of -$CH_3$ and -$CH_2$ increased, too. Thirdly, after the modification, a new N-H stretching vibration peak appeared at about 3136 $cm^{-1}$, signifying the successful introduction of N-H bond into MMEN-ZIF-8, MA-ZIF-8, and ED-ZIF-8 materials. Fourthly, the antisymmetric stretching vibration peaks of -$CH_3$ and -$CH_2$ increased at around 2960 $cm^{-1}$ and 2930 $cm^{-1}$ after the modification, indicating that two groups -$CH_3$ and -$CH_2$ were introduced after modification. In summary, after ZIF-8 materials are modified with different organic amine groups, N-H bonds have been successfully introduced. The thermal stability of amine@ZIF-8 was evaluated by TGA experiment under $N_2$ flow from 30°C to 800°C (see FIGURE S2). It can

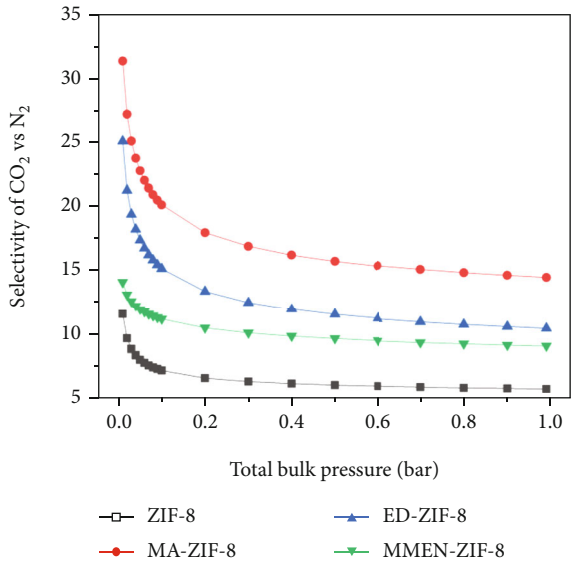


FIGURE 8: The IAST-predicted selectivities for equimolar $CO_2$ and $N_2$ at 298 K as a function of total bulk pressure.

be evidently seen that the modified ZIF-8 materials all had better thermal stability than ZIF-8, while the MA-ZIF-8 was even stable up to 427°C.

### 3.2. $CO_2$ and $N_2$ Adsorption on Amine@ZIF-8 at Ambient Temperature

*3.2.1. $CO_2$ Adsorption Isotherms on Amine@ZIF-8 Materials.* Figure 5 exhibits the $CO_2$ adsorption isotherms of amine@-ZIF-8 materials at different temperatures (298 K, 288 K, and 273 K). Clearly, the $CO_2$ adsorption capacities of amine@-ZIF-8 materials increased dramatically at each temperature. At 298 K, their $CO_2$ amounts adsorbed were in the following way: MA − ZIF − 8 > MMEN − ZIF − 8 > ED − ZIF − 8 > ZIF − 8. Moreover, by comparison with the original ZIF-8, the $CO_2$ adsorption capacities on MA-ZIF-8, MMEN-ZIF-8, and ED-ZIF-8 increased by 118.2%, 90.2%, and 29.8%, respectively. This may be caused by the obvious increase in the BET surface area and micropore pore volume of amine@ZIF-8 materials [52]. In addition, the N-H group introduced would also promote their adsorption performance toward $CO_2$.

*3.2.2. $N_2$ Adsorption Isotherms on Amine@ZIF-8 Materials.* Figure 6 displays the $N_2$ adsorption isotherms on amine@-ZIF-8 materials at different temperatures (298 K, 288 K, and 273 K). It can be observed that the $N_2$ adsorption capacities of amine@ZIF-8 materials significantly increased. And, the order of their adsorption capacity for $N_2$ is as follows: MA − ZIF − 8 > MMEN − ZIF − 8 > ED − ZIF − 8 > ZIF − 8. Moreover, compared with the original ZIF-8 material, the adsorption capacity of MA-ZIF-8, MMEN-ZIF-8, and ED-ZIF-8 for $N_2$ increased by 42.2%, 33.3%, and 15.0%, respectively. The increase might be due to the increased specific surface area and total pore volume after amine modification.

*3.3. Adsorption Selectivity of $CO_2$ vs. $N_2$ on Amine@ZIF-8 at Ambient Temperature.* The ideal adsorbed solution theory (IAST) developed by Myers and Praunitz was proved to be an efficient method to evaluate the adsorption equilibrium of gas mixtures and selectivity using single-component isotherms [45]. Before carrying out the IAST simulation, the single-component adsorption isotherms of $CO_2$ and $N_2$ were separately fitted by the dual-site Langmuir-Freundlich (DSLF) equation (see equation S1).

Figure 7 presents the single-component isotherms and the DSLF fitted ones. Obviously, the DSLF model can be applied favourably to fit the single-component adsorption data. From the fitting parameters listed in Table 2, it can be observed that the correlation coefficients $R^2$ are all up to 0.9999, implying the well fitted single-component isotherms using the DSLF model. Figure 8 exhibits predicted selectivities of amine@ZIF-8 materials as a function of total bulk pressure for equimolar $CO_2$ and $N_2$ mixtures at 298 K. Clearly, the $CO_2/N_2$ selectivity of amine@ZIF-8 materials decreased with the increase of pressure. Moreover, the adsorption selectivities of $CO_2/N_2$ on amine@ZIF-8 materials are always higher than those of ZIF-8, particularly in the low-pressure region. Furthermore, the $CO_2/N_2$ selectivity on MA-ZIF-8 is the highest in the pressure range. And, the $CO_2/N_2$ adsorption selectivities on the amine@ZIF-8 were in the order of MA − ZIF − 8 > ED − ZIF − 8 > MMEN − ZIF − 8 > ZIF − 8. Especially, at 0.01, 0.5, and 1.0 bar, the $CO_2/N_2$ selectivities of MA-ZIF-8 were up to 31, 16, and 14, respectively, which is almost three times of those of the original ZIF-8.

*3.4. Isosteric Heat of Adsorption.* The isosteric heat of adsorption ($Q_{st}$) determines the regeneration temperature of adsorbents used during a PSA or TSA process. The enthalpies of $CO_2$ adsorption (at 273 K, 288 K, and 298 K) on ZIF-8, MA-ZIF-8, ED-ZIF-8, and MMEN-ZIF-8 materials were calculated with the virial method [57, 58]. Figure 9(a) shows the $Q_{st}$ of $CO_2$ on the amine@ZIF-8 materials. Obviously, at the very beginning of adsorption, the $Q_{st}$ values were in the following order: MA − ZIF − 8 > MMEN − ZIF − 8 > ED − ZIF − 8 > ZIF − 8, suggesting a much stronger interaction between $CO_2$ and amine@ZIF-8 frameworks. Besides, the $Q_{st}$ of $CO_2$ evidently decreased with the increase of $CO_2$ amounts adsorbed on the amine@ZIF-8. This phenomenon can be attributed to the surface heterogeneity of the amine@ZIF-8 samples. Figure 9(b) shows that $Q_{st}$ of $N_2$ adsorption on the amine@ZIF-8. As compared to Figure 9(a), it is visible that the $Q_{st}$ of $N_2$ on each of the material was lower than that of $CO_2$, confirming the favorable selectivity of the modified ZIF-8 materials for $CO_2/N_2$. Moreover, the $Q_{st}$ of $N_2$ on the amine@ZIF-8 are all almost independent of the $N_2$ uptake, indicating the weak interaction between $N_2$ and the modified ZIF-8 material. In addition, the $Q_{st}$ of $CO_2$ on ED-ZIF-8, MMEN-ZIF-8, and MA-ZIF-8, respectively, all gets higher, and the $Q_{st}$ of $N_2$ turns lower than that of original ZIF-8 at meantime. As a consequence of that, the $CO_2/N_2$ selectivities of the amine@ZIF-8 all become higher in comparison with those of ZIF-8.

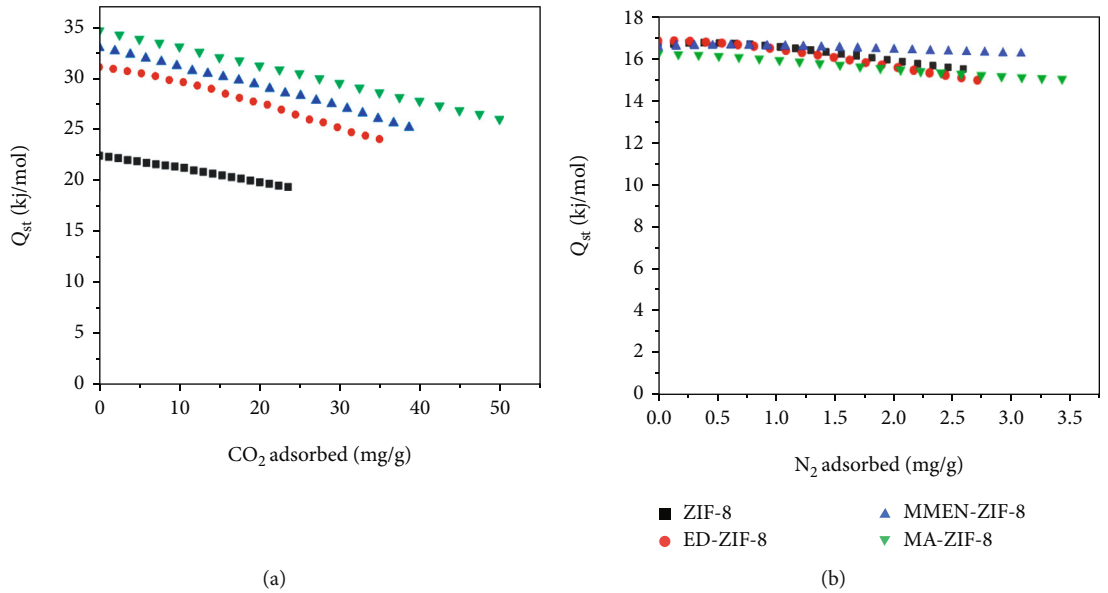


FIGURE 9: Dependence of isosteric heat of adsorption on the amounts adsorbed of $CO_2$ and $N_2$ over the amine@ZIF-8 materials: (a) $CO_2$; (b) $N_2$.

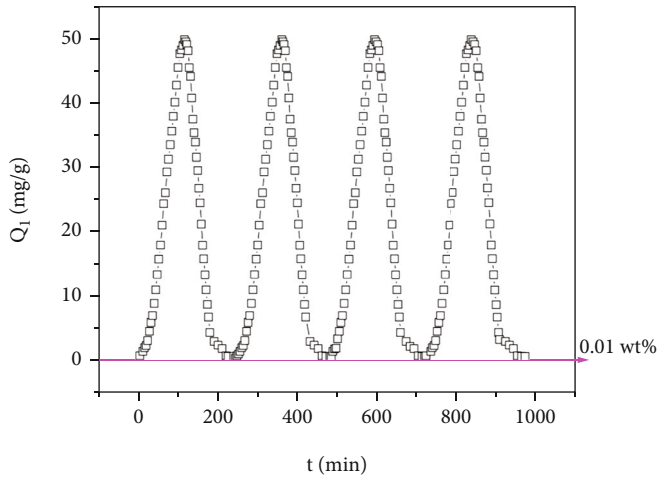


FIGURE 10: Volumetric recycle runs of $CO_2$ adsorption-desorption on the MA-ZIF-8 at 298 K and 1 bar for adsorption and 1 mbar for desorption.

*3.5. Cyclic Adsorption-Desorption Performances of $CO_2$ on MA-ZIF-8 Material.* In order to assess the reusability of $CO_2$ on the modified ZIF-8, we further performed the $CO_2$ adsorption-desorption cycle test on MA-ZIF-8 material. Figure 10 presents the variation curves of $CO_2$ uptake on MA-ZIF-8 material during four continuous cycles of $CO_2$ volumetric adsorption and desorption experiments at 298 K. It can be seen that after four adsorption-desorption cycles, the $CO_2$ desorption efficiency was higher than 99%, and only about 0.01 wt% $CO_2$ remains on the adsorbent. This indicated that the adsorption of $CO_2$ on the MA-ZIF-8 sample was reversible, and the MA-ZIF-8 sample had good regeneration performance. In addition, the shapes of the four adsorption-desorption cycle curves were analogous, denoting that MA-ZIF-8 was very stable and suitable for $CO_2$ adsorption.

Figure 11 presents the six gravimetric $CO_2$ adsorption-desorption cycles for MA-ZIF-8, where the desorption processes were evaluated at 125°C and 150°C, respectively. As it was noted, after each desorption process, an obvious decrease can be observed. Furthermore, when the desorption temperature increased from 125°C to 150°C, there was only a slight variation in the weight of MA-ZIF-8. For MMEN-ZIF-8 and ED-ZIF-8, similar phenomenon can be observed (see Figures S3 and S4). Therefore, the desorption temperature has little effect on the $CO_2$ capture during cycles. It also can be concluded that 125°C is enough for the regeneration of amine@ZIF-8 materials.

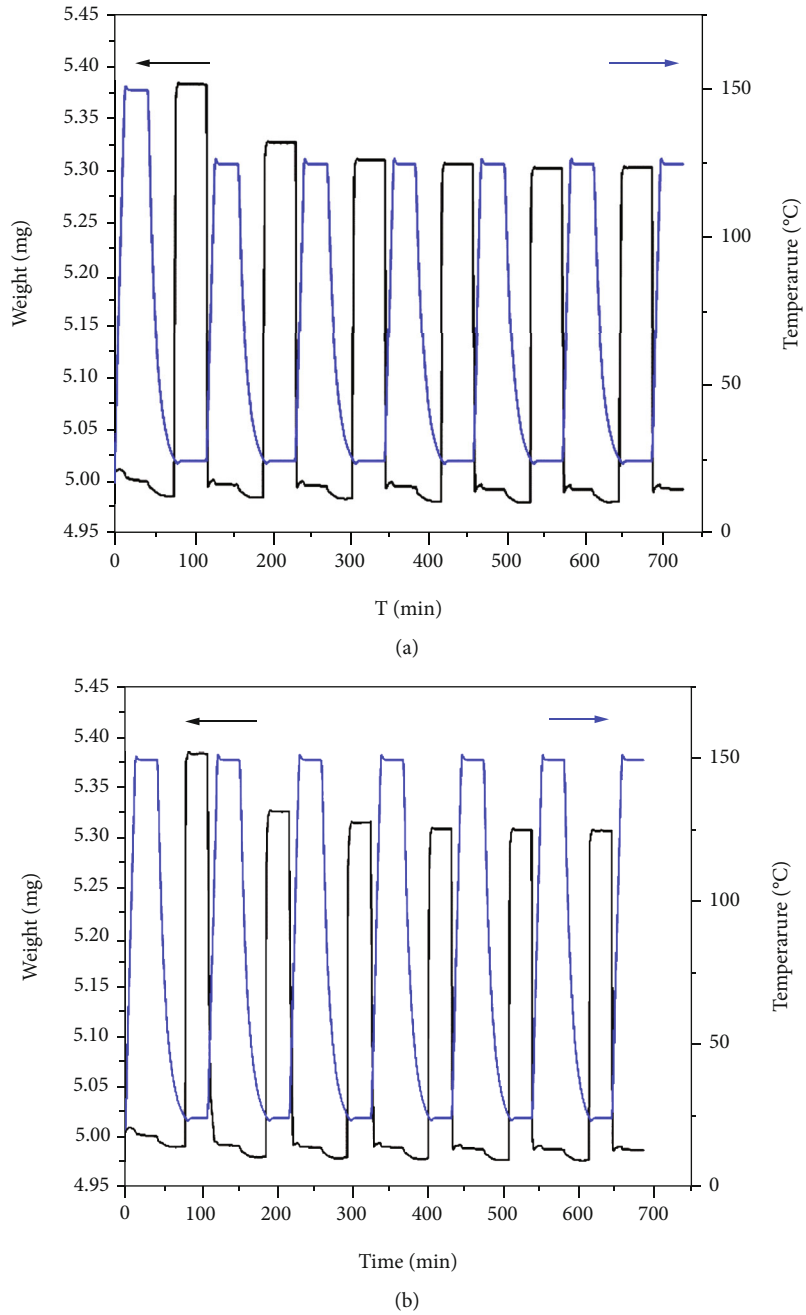


Figure 11: Six gravimetric $CO_2$ adsorption-desorption cycles on the MA-ZIF-8 at 298 K and desorption at 125°C and 150°C, respectively: (a) 125°C; (b) 150°C.

## 4. Conclusions

The as-synthesized ZIF-8 material was successfully modified with methylamine, ethylenediamine, and *N*, *N* ′-dimethylethylenediamine by using a postsynthetic method to enhance its adsorption capacity and selectivity toward $CO_2$. The BET surface areas of MA-ZIF-8, ED-ZIF-8, and MMEN-ZIF-8 increased by 118.2%, 29.8%, and 90.2%, respectively, in comparison with ZIF-8. Moreover, the N-H groups were grafted into the surfaces of the amine-modified samples. In addition, the three amine@ZIF-8 materials (MA-ZIF-8, ED-ZIF-8, and MMEN-ZIF-8) all had higher $CO_2$ adsorption capacities in contrast to ZIF-8 samples, increasing by 110.5%, 49.4%, and 64.8%, respectively. This enhancement was mainly because of their larger surface areas and stronger interaction between $CO_2$ and the Lewis basic amine groups. The IAST theory was employed to predict the adsorption equilibrium and selectivity from the single-component isotherms. The amine@ZIF-8 materials all showed larger $CO_2/N_2$ selectivity than that of ZIF-8, particularly in the low-pressure region. Moreover, at 0.01, 0.5, and 1.0 bar, the selectivities of $CO_2/N_2$ on the MA-ZIF-8 were separately up to 31, 16, and 14, which is almost three times of that of ZIF-8. The $Q_{st}$ of $CO_2$ adsorption on the

MA-ZIF-8, MMEN-ZIF-8, and ED-ZIF-8 all become higher, while, the $Q_{st}$ of $N_2$ on these samples was slightly lower as contrast to that on ZIF-8. Furthermore, six gravimetric $CO_2$ adsorption-desorption recycle runs on MA-ZIF-8, MMEN-ZIF-8, and ED-ZIF-8 indicated the good repeatability and feasibility of the modified ZIF-8 for $CO_2$ capture, highlighting the possibility of using MA-ZIF-8 for industrial $CO_2$ adsorption and separation.

## Data Availability

The data used to support the findings of this study are included within the article.

## Conflicts of Interest

The authors declared no potential conflicts of interest with respect to the research, authorship, and/or publication of this article.

## Acknowledgments

This work was supported by the National Natural Science Foundation of China (21878122), the Pearl River S and T Nova Program of Guangzhou (201710010053), and the Zhengzhou Science and Technology Project (141PPTGG433).

## Supplementary Materials

Concentrations of MA, ED, and MMEN used in the postsynthetic modification processes, DFT pore size distributions, thermal gravimetric analysis, and six gravimetric $CO_2$ adsorption-desorption cycles of the modified ZIF-8 materials are shown in the Supplemental Material. Figure S1: DFT pore size distributions for ZIF-8 and amine-modified ZIF-8 materials. (a) MA@ZIF-8; (b) ED@ZIF-8; (c) MMEN@ZIF-8. Figure S2: thermogravimetric (TG) profiles of ZIF-8 and modified ZIF-8. (a) ZIF-8 and MA samples; (b) ZIF-8 and ED samples. Figure S3: six gravimetric $CO_2$ adsorption-desorption cycles on the MMEN-ZIF-8 at 298 K and desorption at 125°C and 150°C, respectively. (a) 125°C; (b) 150°C. Figure S4: six gravimetric $CO_2$ adsorption-desorption cycles on the ED-ZIF-8 at 298 K and desorption at 125°C and 150°C, respectively. (a) 125°C; (b) 150°C. Table S1: concentration gradients of MA, ED, and MMEN used in the ZIF-8 postmodification process. Table S2: textural properties of the ZIF-8 samples prepared using different synthesis and purification conditions. *(Supplementary Materials)*

## References

[1] M. B. Hahn, A. M. Riederer, and S. O. Foster, "The livelihood vulnerability index: a pragmatic approach to assessing risks from climate variability and change—a case study in Mozambique," *Global Environmental Change*, vol. 19, no. 1, pp. 74–88, 2009.

[2] Z. Li, P. Liu, C. Ou, and X. Dong, "Porous metal–organic frameworks for carbon dioxide adsorption and separation at low pressure," *ACS Sustainable Chemistry & Engineering*, vol. 8, no. 41, pp. 15378–15404, 2020.

[3] J. S. T. Pedersen, F. D. Santos, D. van Vuuren et al., "An assessment of the performance of scenarios against historical global emissions for IPCC reports," *Global Environmental Change*, vol. 66, p. 102199, 2021.

[4] X. Zhang, X. Zhao, Z. Jiang, and S. Shao, "How to achieve the 2030 $CO_2$ emission-reduction targets for China's industrial sector: retrospective decomposition and prospective trajectories," *Global Environmental Change*, vol. 44, pp. 83–97, 2017.

[5] L. A. Darunte, K. S. Walton, D. S. Sholl, and C. W. Jones, "$CO_2$ capture via adsorption in amine-functionalized sorbents," *Current Opinion in Chemical Engineering*, vol. 12, pp. 82–90, 2016.

[6] D. Sun, Y. Fu, W. Liu et al., "Studies on photocatalytic $CO_2$ reduction over $NH_2$-Uio-66(Zr) and its derivatives: towards a better understanding of photocatalysis on metal-organic frameworks," *Chemistry – A European Journal*, vol. 19, no. 42, pp. 14279–14285, 2013.

[7] C. W. Jones, "$CO_2$ capture from dilute gases as a component of modern global carbon management," *Annual Review of Chemical and Biomolecular Engineering*, vol. 2, no. 1, pp. 31–52, 2011.

[8] X. Wu, Y. Yu, Z. Qin, and Z. Zhang, "The advances of post-combustion $CO_2$ capture with chemical solvents: review and guidelines," *Energy Procedia*, vol. 63, pp. 1339–1346, 2014.

[9] M. Harja, R. Tataru-Farmus, D. Hultuana, C. G. . Castro, G. Ciobanu, and L. Lazar, "Influence of ethylenediamine content over performance of $CO_2$ absorption into potassium carbonate solutions," *Environmental Engineering and Management Journal*, vol. 20, no. 4, pp. 507–516, 2021.

[10] F. O. Ochedi, J. Yu, H. Yu, Y. Liu, and A. Hussain, "Carbon dioxide capture using liquid absorption methods: a review," *Environmental Chemistry Letters*, vol. 19, no. 1, pp. 77–109, 2021.

[11] S. R. Shewchuk, A. Mukherjee, and A. K. Dalai, "Selective carbon-based adsorbents for carbon dioxide capture from mixed gas streams and catalytic hydrogenation of $CO_2$ into renewable energy source: a review," *Chemical Engineering Science*, vol. 243, p. 116735, 2021.

[12] D.-i. Kwon, J.-C. Kim, H. Lee, W. Lee, and C. Jo, "Engineering micropore walls of beta zeolites by post-functionalization for $CO_2$ adsorption performance screening under humid conditions," *Chemical Engineering Journal*, vol. 427, p. 131461, 2022.

[13] A. Kumar, D. G. Madden, M. Lusi et al., "Direct air capture of $CO_2$ by physisorbent materials," *Angewandte Chemie International Edition*, vol. 54, no. 48, pp. 14372–14377, 2015.

[14] X. Shi, H. Xiao, H. Azarabadi et al., "Sorbents for the direct capture of $CO_2$ from ambient air," *Angewandte Chemie International Edition*, vol. 59, no. 18, pp. 6984–7006, 2020.

[15] Y.-C. Chiang, C.-C. Huang, and W.-T. Chin, "Carbon dioxide adsorption on carbon nanofibers with different porous structures," *Applied Sciences*, vol. 11, no. 16, p. 7724, 2021.

[16] D. Bahamon, A. Díaz-Márquez, P. Gamallo, and L. F. Vega, "Energetic evaluation of swing adsorption processes for $CO_2$ capture in selected MOFs and zeolites: effect of impurities," *Chemical Engineering Journal*, vol. 342, pp. 458–473, 2018.

[17] Y. Jung, Y. G. Ko, I. W. Nah, and U. S. Choi, "Designing large-sized and spherical $CO_2$ adsorbents for highly reversible $CO_2$

capture and low pressure drop," *Chemical Engineering Journal*, vol. 427, p. 131781, 2022.

[18] C. Wang, S. K. Biswas, and S. Okubayashi, "Polyethyleniminе-impregnated mesoporous delignified wood with high mechanical strength for $CO_2/N_2$ selective adsorption," *ACS Applied Nano Materials*, vol. 3, no. 6, pp. 5499–5508, 2020.

[19] C. Healy, K. Patil, B. Wilson et al., "The thermal stability of metal-organic frameworks," *Coordination Chemistry Reviews*, vol. 419, p. 213388, 2020.

[20] H. Zhang, J. Nai, L. Yu, and X. Lou, "Metal-organic-framework-based materials as platforms for renewable energy and environmental applications," *Joule*, vol. 1, no. 1, pp. 77–107, 2017.

[21] A. A. Olajire, "Synthesis chemistry of metal-organic frameworks for $CO_2$ capture and conversion for sustainable energy future," *Renewable and Sustainable Energy Reviews*, vol. 92, pp. 570–607, 2018.

[22] R. Banerjee, A. Phan, B. Wang et al., "High-throughput synthesis of zeolitic imidazolate frameworks and application to $CO_2$ capture," *Science*, vol. 319, no. 5865, pp. 939–943, 2008.

[23] T. Ghanbari, F. Abnisa, and W. M. A. Wan Daud, "A review on production of metal organic frameworks (MOF) for $CO_2$ adsorption," *Science of the Total Environment*, vol. 707, p. 135090, 2020.

[24] J. Gascon, A. Corma, F. Kapteijn, and F. X. Llabres i Xamena, "Metal organic framework catalysis: quo vadis?," *ACS Catalysis*, vol. 4, no. 2, pp. 361–378, 2014.

[25] B. Li, H.-M. Wen, Y. Cui, W. Zhou, G. Qian, and B. Chen, "Emerging multifunctional metal–organic framework materials," *Advanced Materials*, vol. 28, no. 40, pp. 8819–8860, 2016.

[26] X. Zhang, G. Li, D. Wu et al., "Recent progress in the design fabrication of metal-organic frameworks-based nanozymes and their applications to sensing and cancer therapy," *Biosensors and Bioelectronics*, vol. 137, pp. 178–198, 2019.

[27] S. Wang, C. Wang, and Q. Zhou, "Strong foam-like composites from highly mesoporous wood and metal-organic frameworks for efficient CO2Capture," *ACS Applied Materials & Interfaces*, vol. 13, no. 25, pp. 29949–29959, 2021.

[28] D. Chong, Z. Jawad, P. C. Tan, and M. Abed, "The influence of blending different molecular weights of cellulose acetate butyrate for $CO_2/N_2$ separation," *Journal of Physical Science*, vol. 31, no. 2, pp. 91–112, 2020.

[29] H. R. Abid, Z. H. Rada, L. Liu, S. Wang, and S. Liu, "Striking $CO_2$ capture and $CO_2/N_2$ separation by Mn/Al bimetallic MIL-53," *Polyhedron*, vol. 193, p. 114898, 2021.

[30] J.-M. Liu, J.-X. Hou, J. Liu, X. Jing, L. J. Li, and J. L. du, "Pyrazinyl-functionalized Zr(IV)-MOF for ultrasensitive detection of tyrosine/TNP and efficient $CO_2/N_2$separation," *Journal of Materials Chemistry C*, vol. 7, no. 38, pp. 11851–11857, 2019.

[31] B. Yu, H. Yu, Q. Yang et al., "Postcombustion capture of $CO_2$ by diamines containing one primary and one tertiary amino group: reaction rate and mechanism," *Energy & Fuels*, vol. 33, no. 8, pp. 7500–7508, 2019.

[32] Z. Hu, Y. Wang, B. B. Shah, and D. Zhao, "CO2Capture in Metal-Organic Framework Adsorbents: An Engineering Perspective," *Advanced Sustainable Systems*, vol. 3, no. 1, 2019.

[33] M. Ding, R. Flaig, H.-L. Jiang, and O. Yaghi, "Carbon capture and conversion using metal–organic frameworks and MOF-based materials," *Chemical Society reviews*, vol. 48, no. 10, pp. 2783–2828, 2019.

[34] L. T. Oliveira, R. V. Gonçalves, D. V. Gonçalves, D. C. S. de Azevedo, and S. M. Pereira de Lucena, "Superior performance of mesoporous MOF MIL-100 (Fe) impregnated with ionic liquids for $CO_2$ adsorption," *Journal of Chemical & Engineering Data*, vol. 64, no. 5, pp. 2221–2228, 2019.

[35] T. K. Vo, P. V. Vu, V. C. Nguyen, and J. Kim, "Construction of OH sites within MIL-101 (Cr)-NH2 framework for enhanced $CO_2$ adsorption and $CO_2/N_2$ selectivity," *Korean Journal of Chemical Engineering*, vol. 38, no. 8, pp. 1676–1685, 2021.

[36] M. Zeeshan, H. Gulbalkan, Z. Haşlak, S. Keskin, and A. Uzun, "Doubling $CO_2/N_2$ separation performance of CuBTC by incorporation of 1- *n* -ethyl-3-methylimidazolium diethyl phosphate," *Microporous and Mesoporous Materials*, vol. 316, p. 110947, 2021.

[37] M. Younas, M. Rezakazemi, M. Daud et al., "Recent progress and remaining challenges in post-combustion $CO_2$ capture using metal-organic frameworks (MOFs)," *Progress in Energy and Combustion Science*, vol. 80, p. 100849, 2020.

[38] S. Kazemi and V. Safarifard, "Carbon dioxide capture in MOFs: the effect of ligand functionalization," *Polyhedron*, vol. 154, pp. 236–251, 2018.

[39] X.-J. Gao and H.-G. Zheng, "The difference in the $CO_2$ adsorption capacities of different functionalized pillar-layered metal–organic frameworks (MOFs)," *Dalton Transactions*, vol. 50, no. 26, pp. 9310–9316, 2021.

[40] X. He, D.-R. Chen, and W.-N. Wang, "Bimetallic metal-organic frameworks (MOFs) synthesized using the spray method for tunable $CO_2$ adsorption," *Chemical Engineering Journal*, vol. 382, p. 122825, 2020.

[41] N. Li, Z. Chang, H. Huang et al., "Specific K+Binding sites as CO2Traps in a porous MOF for enhanced CO2Selective sorption," *Small*, vol. 15, no. 22, p. 1900426, 2019.

[42] J. Zhu, L. Wu, Z. Bu, S. Jie, and B.-G. Li, "Polyethyleneimine-modified UiO-66-$NH_2$(Zr) metal–organic frameworks: preparation and enhanced $CO_2$ selective adsorption," *ACS Omega*, vol. 4, no. 2, pp. 3188–3197, 2019.

[43] M. Babar, M. Mubashir, A. Mukhtar et al., "Sustainable functionalized metal-organic framework $NH_2$-MIL-101(Al) for $CO_2$ separation under cryogenic conditions," *Environmental Pollution*, vol. 279, p. 116924, 2021.

[44] Y.-J. Zhang, H.-X. Nie, M.-H. Yu, and Z. Chang, "Post-synthetic modification of tetrazine functionalized porous MOF for $CO_2$ sorption performances modulation," *Journal of Solid State Chemistry*, vol. 300, p. 122257, 2021.

[45] Z. Zhang, S. Xian, Q. Xia, H. Wang, Z. Li, and J. Li, "Enhancement of $CO_2$ adsorption and $CO_2/N_2$ selectivity on ZIF-8 via postsynthetic modification," *AICHE Journal*, vol. 59, no. 6, pp. 2195–2206, 2013.

[46] J. Lim, S. Lee, H. Ha et al., "Amine-tagged fragmented ligand installation for covalent modification of MOF-74," *Angewandte Chemie International Edition*, vol. 60, no. 17, pp. 9296–9300, 2021.

[47] Z. H. Rada, H. R. Abid, J. Shang et al., "Effects of amino functionality on uptake of $CO_2$, $CH_4$ and selectivity of $CO_2/CH_4$ on titanium based MOFs," *Fuel*, vol. 160, pp. 318–327, 2015.

[48] Z. Qiao, N. Wang, J. Jiang, and J. Zhou, "Design of amine-functionalized metal–organic frameworks for $CO_2$ separation: the more amine, the better?," *Chemical Communications*, vol. 52, no. 5, pp. 974–977, 2016.

[49] A. Justin, J. Espín, I. Kochetygov, M. Asgari, O. Trukhina, and W. L. Queen, "A two step postsynthetic modification strategy:

appending short chain polyamines to Zn-NH2-BDC MOF for enhanced $CO_2$ adsorption," *Inorganic Chemistry*, vol. 60, no. 16, pp. 11720–11729, 2021.

[50] Y. Xia, Y. Hong, R. Geng et al., "Amine-functionalized ZIF-8 as a fluorescent probe for breath volatile organic compound biomarker detection of lung cancer patients," *ACS Omega*, vol. 5, no. 7, pp. 3478–3486, 2020.

[51] Z. Zhang, S. Xian, H. Xi, H. Wang, and Z. Li, "Improvement of $CO_2$ adsorption on ZIF-8 crystals modified by enhancing basicity of surface," *Chemical Engineering Science*, vol. 66, no. 20, pp. 4878–4888, 2011.

[52] E. García-Díez, S. Schaefer, A. Sanchez-Sanchez et al., "Novel porous carbons derived from coal tar rejects: assessment of the role of pore texture in $CO_2$ capture under realistic post-combustion operating temperatures," *ACS Applied Materials & Interfaces*, vol. 11, no. 40, pp. 36789–36799, 2019.

[53] E. García-Díez, A. Castro-Muñiz, J. I. Paredes, M. M. Maroto-Valer, F. Suárez-García, and S. García, "$CO_2$ capture by novel hierarchical activated ordered micro-mesoporous carbons derived from low value coal tar products," *Microporous and Mesoporous Materials*, vol. 318, p. 110986, 2021.

[54] K. S. Park, Z. Ni, A. P. Côté et al., "Exceptional chemical and thermal stability of zeolitic imidazolate frameworks," *Proceedings of the National Academy of Sciences*, vol. 103, no. 27, pp. 10186–10191, 2006.

[55] A. D. Burrows, L. K. Cadman, W. J. Gee, H. A. Hamzah, J. V. Knichal, and S. Rochat, "Tuning the Properties of Metal-Organic Frameworks by Post-synthetic Modification," in *Metal-Organic Frameworks-Applications in Separations and Catalysis*, H. Carcia and S. Navalón, Eds., Wiley-VCH, 2018.

[56] L.-J. Li, P.-Q. Liao, C.-T. He et al., "Grafting alkylamine in UiO-66 by charge-assisted coordination bonds for carbon dioxide capture from high-humidity flue gas," *Journal of Materials Chemistry A*, vol. 3, no. 43, pp. 21849–21855, 2015.

[57] L. Czepirski and J. JagieŁŁo, "Virial-type thermal equation of gas–solid adsorption," *Chemical Engineering Science*, vol. 44, no. 4, pp. 797–801, 1989.

[58] D. Britt, H. Furukawa, B. Wang, T. G. Glover, and O. M. Yaghi, "Highly efficient separation of carbon dioxide by a metal-organic framework replete with open metal sites," *Proceedings of the National Academy of Sciences*, vol. 106, no. 49, pp. 20637–20640, 2009.